NASA TECHNICAL NOTE

NASA TN D-4683

GAMMA RAY ANGULAR CORRELATIONS FOLLOWING INELASTIC SCATTERING OF 42-MeV ALPHA PARTICLES FROM MAGNESIUM 24

by Regis F. Leonard, William M. Stewart, Norton Baron, and Richard C. Braley

Lewis Research Center
Cleveland, Ohio

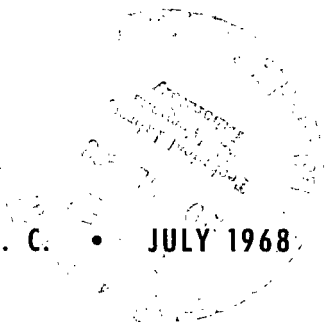

NATIONAL AERONAUTICS AND SPACE ADMINISTRATION • WASHINGTON, D. C. • JULY 1968

NASA TN D-4683

GAMMA RAY ANGULAR CORRELATIONS FOLLOWING INELASTIC SCATTERING OF 42-MeV ALPHA PARTICLES FROM MAGNESIUM 24

By Regis F. Leonard, William M. Stewart, Norton Baron, and Richard C. Braley

Lewis Research Center
Cleveland, Ohio

NATIONAL AERONAUTICS AND SPACE ADMINISTRATION

For sale by the Clearinghouse for Federal Scientific and Technical Information
Springfield, Virginia 22151 – CFSTI price $3.00

ABSTRACT

The angular correlation between inelastically scattered 42-MeV alpha particles and gamma rays emitted in the subsequent nuclear decay has been studied for the 1.37-MeV state of magnesium 24. The symmetry angle of the gamma distribution and the magnitude of the anisotropy of the gamma distribution have been measured for alpha scattering angles between 30° and 76°. The results are compared with the distorted-wave predictions and with the adiabatic and Wills-Cramer models. Observed symmetry angles do not display the large excursions away from the adiabatic line which were seen in earlier work on magnesium 24 at lower energies and more forward angles.

GAMMA RAY ANGULAR CORRELATIONS FOLLOWING INELASTIC SCATTERING OF 42-MeV ALPHA PARTICLES FROM MAGNESIUM 24

by Regis F. Leonard, William M. Stewart, Norton Baron, and Richard C. Braley

Lewis Research Center

SUMMARY

The angular correlation between inelastically scattered 42-MeV alpha particles and gamma rays emitted in the subsequent nuclear decay has been measured for scattering with excitation of the 1.37-MeV level of magnesium 24. The symmetry angle of the gamma distribution and the ratio of isotropic to anisotropic components have been measured for alpha scattering angles between 30° and 76°. The results are compared with the predictions of a distorted-wave Born calculation, as well as with the simpler plane wave, adiabatic, and the Wills-Cramer model predictions. The experimentally observed symmetry angles were relatively close to the adiabatic prediction over the range of alpha particle scattering angles studied here. This is in strong contrast to the behavior observed for 22-MeV scattering and at angles forward of 30° for 42-MeV scattering, where large (45°) excursions from the adiabatic prediction were seen. Distorted-wave Born approximation calculations were performed using a wide range of optical potentials, only one of which produced any significant difference in the predicted value of the symmetry angle, and none of which predicted any significant difference in the ratio of isotropic to anistropic components (A/B).

INTRODUCTION

The inelastic scattering of medium energy alpha particles is a useful tool for the investigation of collective modes of excitation of nuclei. Several theories are capable of predicting, with fairly reliable results, the differential cross sections for elastic scattering and for many types of inelastic scattering. The differential cross section, however, is not the measurable quantity which is most sensitive to the details of the calculation. The differential cross section involves only the sums of squares of transition amplitudes so that the phases of the transition amplitudes are unimportant to the calcu-

lation. A quantity which is sensitive to not only the magnitudes but also the phases is the angular correlation between the inelastically scattered alpha and the gamma ray emitted in the subsequent decay of the target nucleus (see section THEORY). The present study has measured this correlation as a function of the scattered alpha angle for gamma angles in the plane of the original scattering. Some work of this sort has been done on magnesium 24 (^{24}Mg) at the considerably lower energy of 22 MeV (ref. 1) as well as at 42 MeV (refs. 2 and 3). The work reported herein is compared with that previously reported at 22 MeV and will considerably extend that which has previously been published at 42 MeV. The results of the present experiment are compared with the predictions of the optical model (ref. 4) and distorted-wave Born approximation (ref. 5). In addition, the predictions of Blair's adiabatic model of inelastic scattering (ref. 6) are discussed as well as the results of a model of Wills and Cramer (ref. 7), proposed specifically in order to explain alpha-gamma correlation data observed at 22 MeV.

The present work is concerned only with the excitation of the first (2^+) state of ^{24}Mg. This state and this target were chosen because of the relatively high excitation energy (1.37 MeV) and the relatively large cross section for its excitation. In addition, as previously mentioned, some data were already available which should provide an interesting comparison.

SYMBOLS

A	magnitude of isotropic component of alpha-gamma correlation function
a_s	diffuseness of surface interaction form factor
B	magnitude of anisotropic component of alpha-gamma correlation function
$\frac{d\sigma^{1.37}}{d\sigma^0}$	ratio of cross section for inelastic to that for elastic scattering
$F_L(k_f r)$	amplitude of L^{th} partial outgoing distorted wave
$F_{L_1 \mu_1}$	reduced transition amplitude
$F_\ell(k_i r)$	amplitude of ℓ^{th} partial incoming distorted wave
$\langle j_1 m_1 j_2 m_2 \vert JM \rangle$	Clebsch-Gordan coefficient for addition of angular momenta $j_1 m_1$ and $j_2 m_2$ to obtain a resultant JM
k_f	center-of-mass wave number for outgoing wave
k_i	center-of-mass wave number for incident wave

L_1	angular momentum transfer
N_0	number of elastic events in coincidence spectrum
$N_R^{1.37}$	number of chance coincidences involving inelastically scattered alphas
R_s	radius of surface interaction form factor
T_{fi}	transition amplitude for inelastic scattering
$U_{opt}(r)$	spherical part of optical potential
V	strength of real part of nuclear optical potential
V_o	strength of surface interaction form factor
V_1	nonspherical part of optical potential
$v_L(r)$	surface interaction form factor
W	strength of imaginary part of nuclear optical potential
$W(\theta_\gamma)$	correlation pattern in reaction plane
α, β, γ	parameters used in fitting correlation data, after correction for finite geometry
α', β', γ'	parameters used in fitting correlation data, before correction for finite geometry
θ_o	symmetry angle of alpha-gamma correlation function
θ_α	scattering angle for alpha particles in center-of-mass system
θ_γ	angle of emission of gamma ray, relative to incident beam direction
λ	multipolarity of γ-ray deexcitation
μ_1	projection of angular momentum onto z-axis
φ_f	wave function of target nucleus after inelastic scattering
φ_i	wave function of target nucleus before inelastic scattering
φ_γ	azimuthal angle of emission of gamma ray, relative to plane of original scattering
$\chi_f^{(-)}$	outgoing distorted wave in distorted-wave calculation
$\chi_i^{(+)}$	incoming distorted wave in distorted-wave calculation

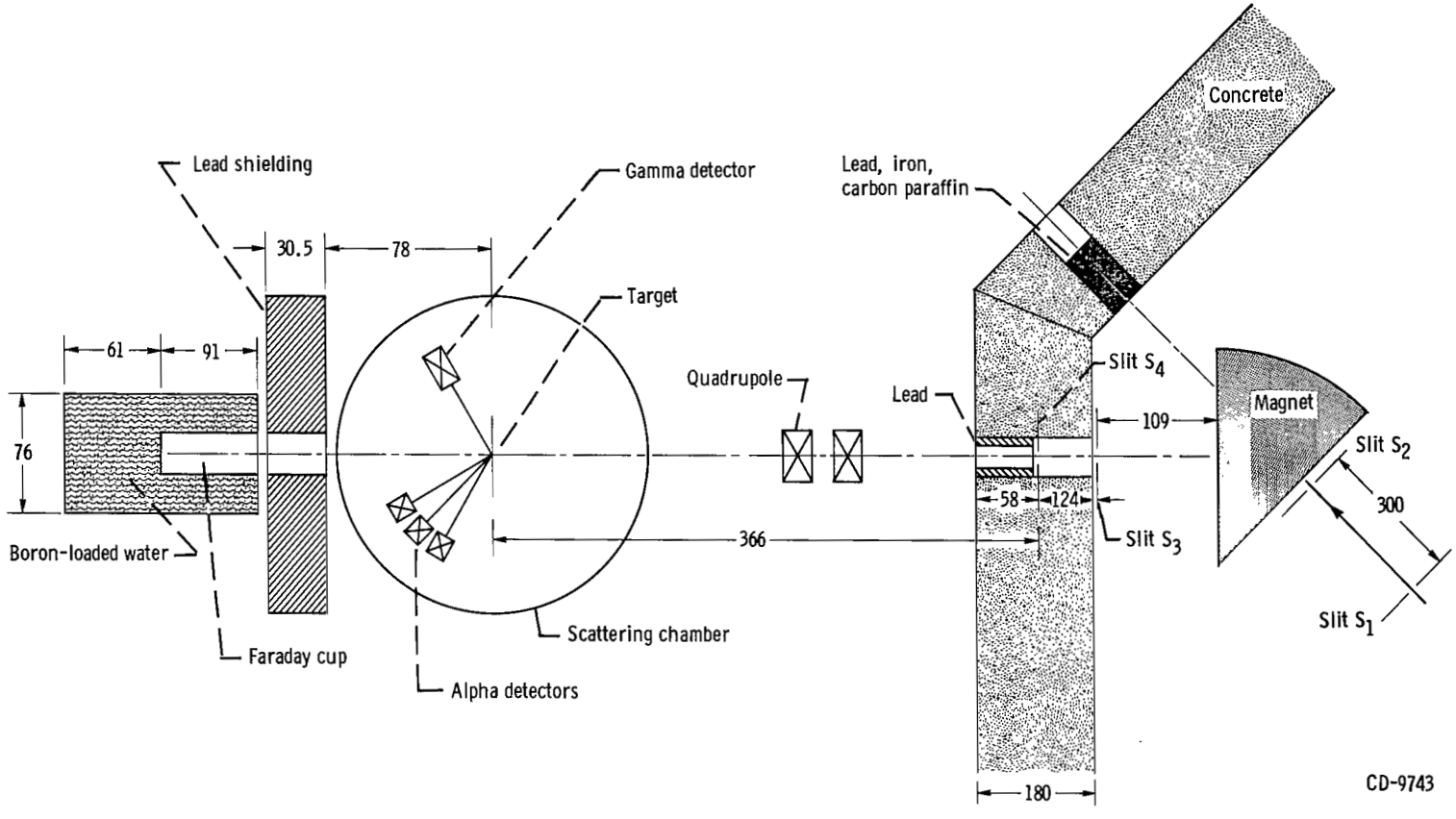

Figure 1. - Schematic diagram of scattering system. (All dimensions are in centimeters.)

EXPERIMENTAL ARRANGEMENT

Beam Handling

The external 42-MeV beam of the NASA 1.5-meter cyclotron was used in this experiment. The considerations used in the overall design of the system were aimed mainly at reducing the background of neutrons and gamma rays present in the beam room. The energy resolution which could be attained in analysis of scattered alpha particles was of secondary interest. An overall schematic diagram of the beam transport system and the experimental area is shown in figure 1. The beam emerging from the cyclotron was focused onto slit S_1, which acted as a source slit for the 45° magnet. The magnet served in the present experiment principally to bend the beam away from the original line, thereby preventing neutrons which emerged from the cyclotron along the original beam line from entering the target area. Slit S_3, which was located 109 centimeters from the exit of the magnet, was ordinarily set to a width of about 1 millimeter and together with S_4, which was 1.5 millimeters wide, defined the direction of the beam incident on the target. Again, for the reduction of the gamma ray background in the target area, the slit S_4 was located approximately 58 centimeters within the concrete wall and backed with a cylinder of lead, 58 centimeters in length, with a 1.9-centimeter-diameter hole to permit passage of the incident beam. Slit S_4, the last defining aperture which the beam passes before reaching the target, was approximately 366 centimeters from the target and the gamma detector. The other principal source of background was the beam stopper. For this, a tank filled with boron-doped water was employed. A Faraday cup was located at the center of the tank. An additional shield of approximately 30.5 centimeters of lead and/or concrete was erected in front of the beam catcher to protect the scattering chamber from the direct radiation from the Faraday cup.

Detectors

Charged-particle detection was supplied by lithium-drifted-silicon solid-state detectors, which were produced at the Lewis Research Center (ref. 8). Three detectors were employed simultaneously, in a four-detector mount which was previously described (ref. 9). For the present experiment, the full angular resolution was 1°. The scattering angle was known to $\pm 0.06^{\circ}$.

Gamma rays were detected by a 7.62- by 7.62-centimeter sodium iodide (Tl) crystal. The distance of the front face of the detector from the target was 12.7 centimeters, so that the full angle subtended by the detector was about 35°; the detector covered about

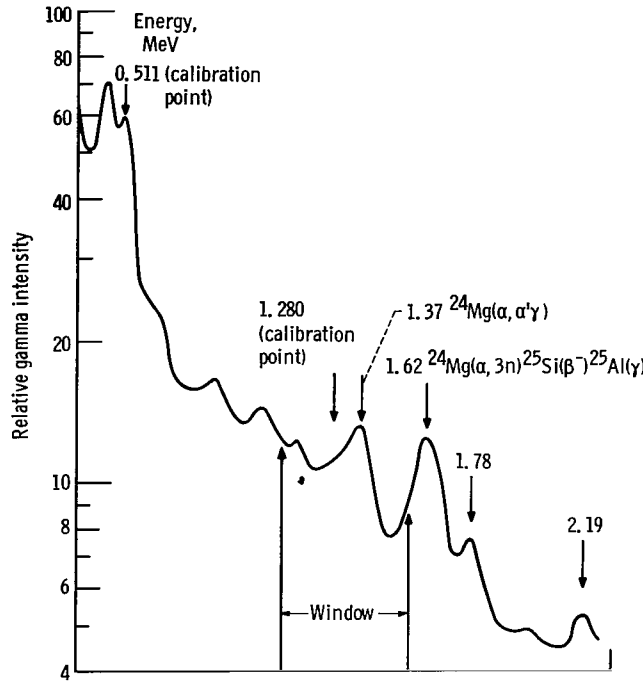

Figure 2. - Gamma ray singles spectrum from the reaction ^{24}Mg(α, γ).

2.2 percent of the total sphere. The gamma spectrum obtained by bombarding the ^{24}Mg target is shown in figure 2.

Electronics

The electronics employed were for the most part commercially available units. A schematic diagram of the electronics is shown in figure 3. Signals from each particle preamplifier passed through a linear amplifier, operated in its double delay line mode, and then through a linear gate, which opened only if the proper coincidence requirements were satisfied. The coincidence requirements were provided by the gamma detector, the signal from which was fanned out to three separate coincidence circuits, one for each particle detector. The individual coincidence circuits were fairly standard parallel fast-slow arrangements. The slow coincidence circuit for each detector required an output from the gamma ray single-channel analyzer, which triggered only on the occurrence of a 1.37-MeV gamma ray. The particle single-channel analyzers on the other hand were used as discriminators to prevent analysis of extremely low energy radiation. The resolving times of the three fast coincidence circuits were 50 nanoseconds, which is less than the time (90 nsec) between cyclotron beam bursts.

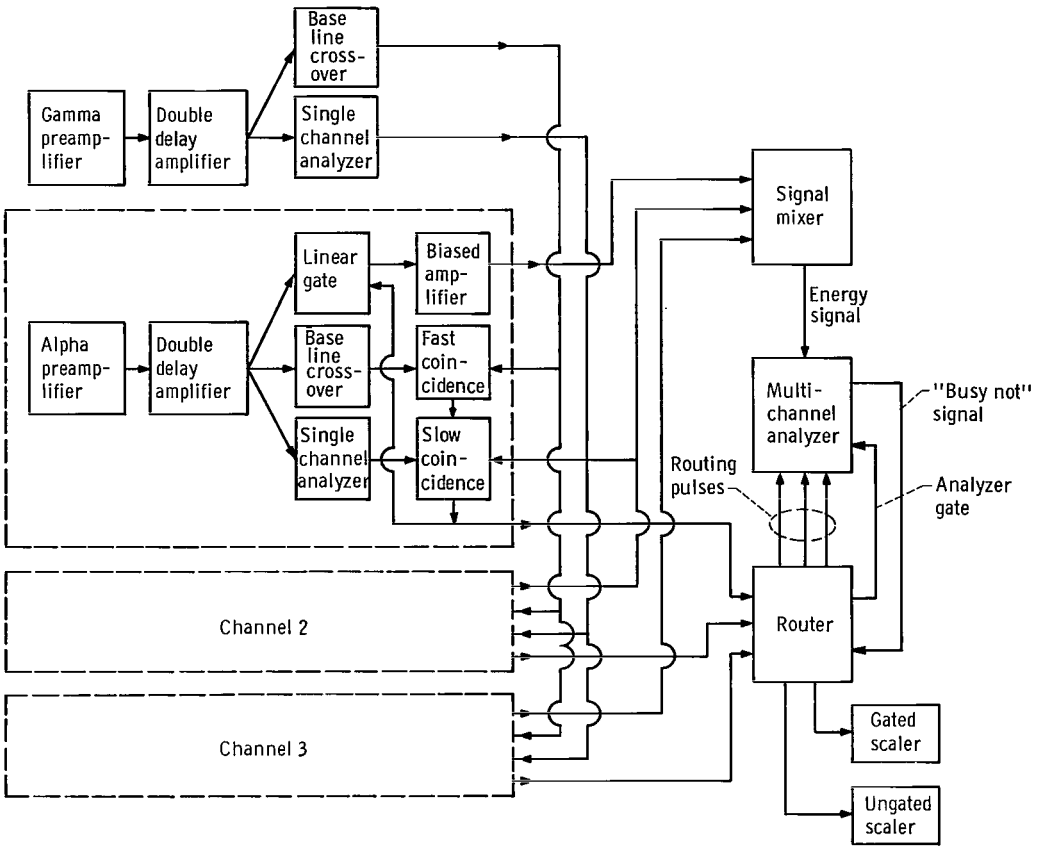

Figure 3. - Block diagram of electronics.

The outputs from each of the particle linear gates were passed through biased amplifiers and then routed to the appropriate quadrant of a 4096 channel pulse height analyzer.

TREATMENT OF EXPERIMENTAL DATA

Data-Taking Procedures

Data were taken over the angular ranges $45^{\circ} \leq \theta_{\gamma} \leq 135^{\circ}$ and $30^{\circ} \leq \theta_{\alpha}^{(lab)} \leq 76^{\circ}$. The gamma detector was moved in 15° steps, making seven gamma angles for each alpha angle. Data were obtained for every 2° of alpha angle.

Since it was necessary to know the ratio of the 1.37-MeV inelastic cross section to the elastic cross section, an alpha particle singles spectrum was taken before and after every coincidence run to provide a continuous monitoring of this quantity and guard

against possible changes caused by small shifts in the direction of the incident beam. By averaging the results obtained before and after a coincidence run it was possible to obtain a ratio which was accurate to better than 5 percent.

Coincidence runs lasted an average of 4 to 6 hours at a beam current of approximately 20 nanoamperes. This current resulted in a true to chance coincidence ratio of between 1:1 and 4:1. Increasing the beam current to 35 nanoamperes caused this ratio to fall to between 1:1 and 1:3. As a result, the time required to obtain a given statistical accuracy could not be decreased by increasing the beam current. For most of the experiment, a true to chance ratio of about 2:1 was maintained.

Reduction of Raw Data

The raw data for this experiment consisted of energy spectra of scattered alpha particles, taken both with and without the requirement that they be in coincidence with a 1.37-MeV gamma ray. Typical results are shown in figure 4. The total intensity of the inelastically scattered alpha particles was determined by simply summing the appropriate analyzer channels. For the coincidence spectra, however, this intensity had

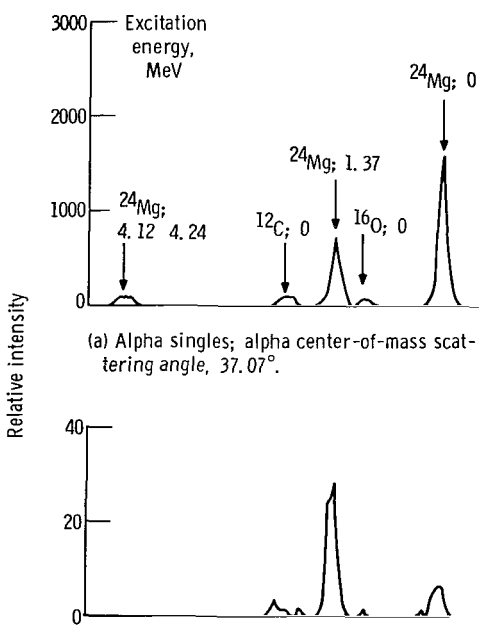

(a) Alpha singles; alpha center-of-mass scattering angle, 37.07°.

(b) Alpha particles in coincidence with 1.37-MeV gamma; alpha center-of-mass scattering angle, 37.07°; emission angle of gamma ray, 120°.

Figure 4. - Typical spectra of alpha particles scattered from magnesium 24.

to be corrected for accidental coincidences. Since in the coincidence spectra all elastically scattered alpha particles were accidental, the number of chance coincidences of inelastically scattered alpha particles was determined by the relation

$$N_R^{1.37} = \frac{d\sigma^{1.37}}{d\sigma^0} N_0 \tag{1}$$

where

$\frac{d\sigma^{1.37}}{d\sigma^0}$ ratio of cross section for inelastic to that for elastic scattering

$N_R^{1.37}$ number of random coincidences involving inelastically scattered alpha particles

N_0 number of elastic events in coincidence spectrum

Fitting of Raw Data

For the sequence of spins investigated herein ($0^+ \rightarrow 2^+ \rightarrow 0^+$) the form of the correlation pattern $W(\theta_\gamma)$ in the reaction plane for a fixed alpha scattering angle is known to be (see section THEORY)

$$W(\theta_\gamma) = A + B \sin^2 2(\theta_\gamma - \theta_0) \tag{2}$$

In this expression and elsewhere in this report, the coordinate system is spherical with the polar axis along the incident beam direction and the azimuthal angle measured from the plane determined by the scattered alpha particle. All gamma ray measurements reported herein are for the azimuthal angle $\varphi_\gamma = \pi$. The measured correlation patterns were fitted to the function of equation (2) by the method of least squares. In order to permit a linear least squares fitting program to be employed, the correlation pattern was rewritten as

$$W(\theta_\gamma) = \alpha' + \beta' \cos 4\theta_\gamma + \gamma' \sin 4\theta_\gamma \tag{3}$$

and the parameters α', β', and γ' were determined. Typical experimental patterns and fits are shown in figure 5.

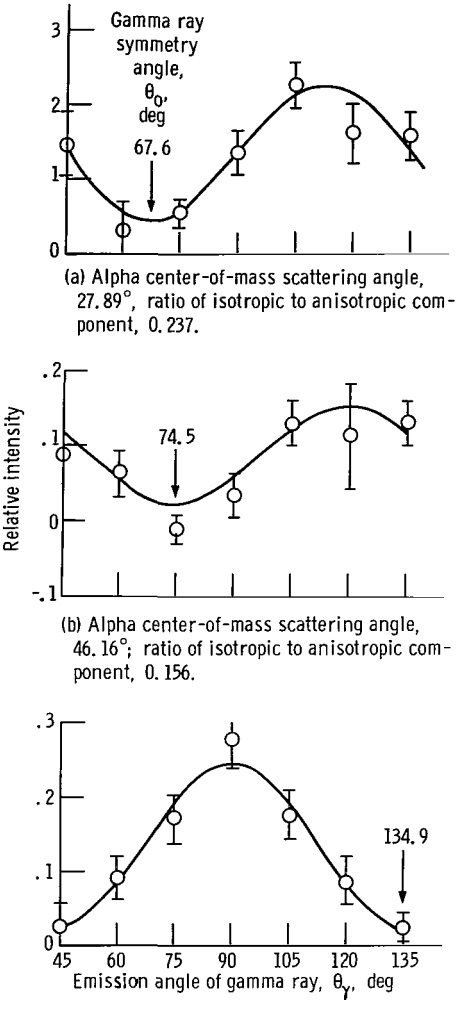

(a) Alpha center-of-mass scattering angle, 27.89°, ratio of isotropic to anisotropic component, 0.237.

(b) Alpha center-of-mass scattering angle, 46.16°; ratio of isotropic to anisotropic component, 0.156.

(c) Alpha center-of-mass scattering angle, 68.31°; ratio of isotropic to anisotropic component, 0.128.

Figure 5. - Typical correlation patterns. Ratios of isotropic to anisotropic component as presented were not corrected for finite geometry.

The parameters determined by this method were corrected for the effects of the finite geometry of the gamma detector by the method of Rose (ref. 10). The actual calculation of the correction was performed by Eidson, Cramer, Blatchley, and Bent (ref. 1) for the exact energy (1.37 MeV) and geometry (7.62- by 7.62-cm detector 12.7 cm from the target) employed here. The true parameters α, β, and γ are given by

TABLE I. - MAGNESIUM 24 $(\alpha, \alpha', \gamma)$ EXPERIMENTAL RESULTS (AFTER CORRECTIONS FOR FINITE GEOMETRY)

Alpha center-of-mass scattering angle, θ_α (cm), deg	Gamma ray symmetry angle, θ_0, deg	Ratio of isotropic to anisotropic component, A/B
27.89	67.6±2.6	0.139±0.08
32.49	65.4±7.5	1.25 ±0.80
34.79	65.8±3.2	.037±0.08
37.07	66.9±2.0	.070±0.06
39.36	63.9±2.5	.120±0.08
41.63	63.1±2.5	.127±0.07
43.90	68.0±2.3	.181±0.07
46.16	74.5±4.5	.073±0.12
48.41	54.0±3.5	0 ±0.1
50.66	57.6±3.0	0 ±0.07
52.90	56.0±5.8	.233±0.18
55.13	55.2±8.0	1.17 ±2.0
57.35	58.5±3.8	0 ±0.07
59.56	60.1±1.8	.002±0.05
61.76	60.8±4.5	.170±0.14
63.95	51.5±2.0	.138±0.06
66.14	45.9±3.3	0 ±0.09
68.31	44.9±2.0	.044±0.05
70.47	41.5±2.3	0 ±0.13
72.63	49.9±3.2	.280±0.10
74.77	61.9±2.6	0 ±0.08
76.90	50.5±6.0	.200±0.18
79.02	61.7±5.6	.482±0.26
81.13	34.4±4.5	.097±0.12
83.23	43.3±5.5	.346±0.17
85.32	38.2±9.5	.223±0.30

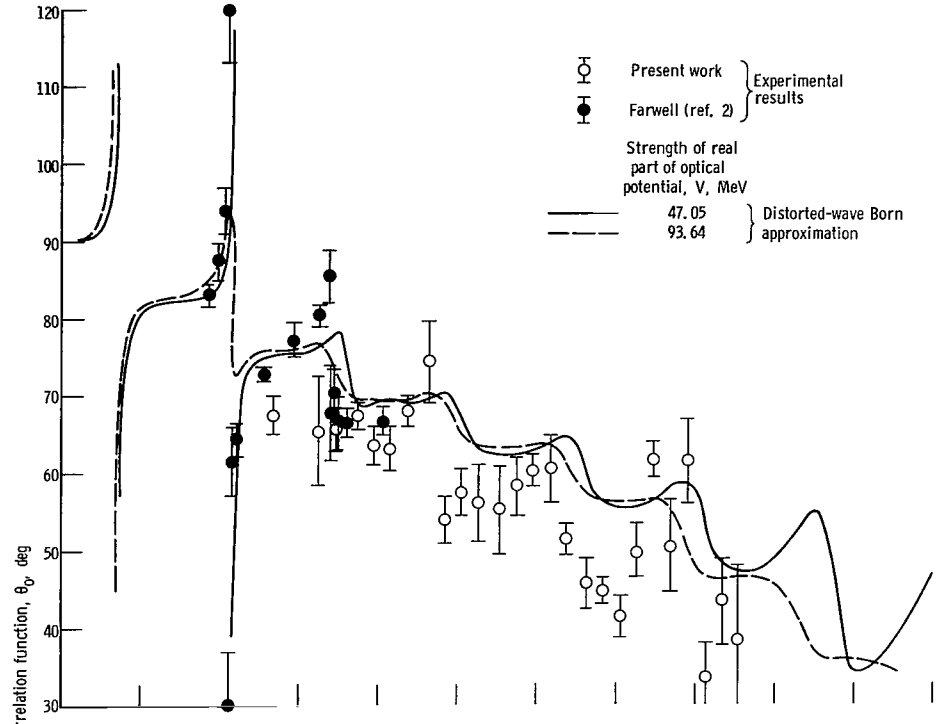

(a) First and second sets of optical potentials.

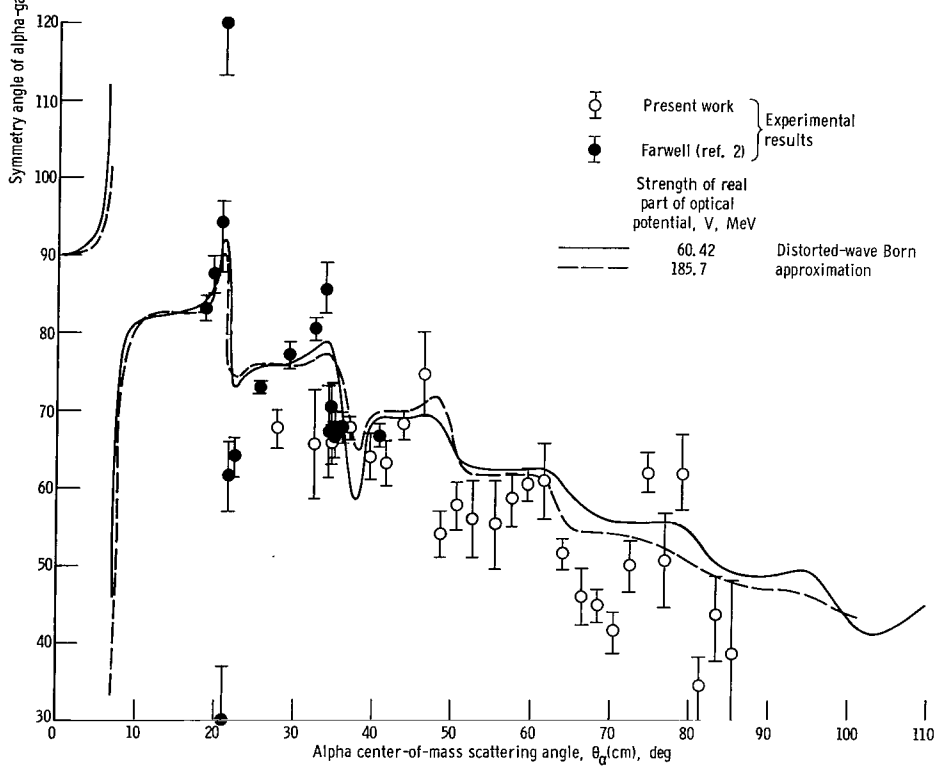

(b) Third and fourth sets of optical potentials.

Figure 6. - Gamma ray symmetry angle for the reaction $^{24}Mg(\alpha, \alpha'\gamma)$.

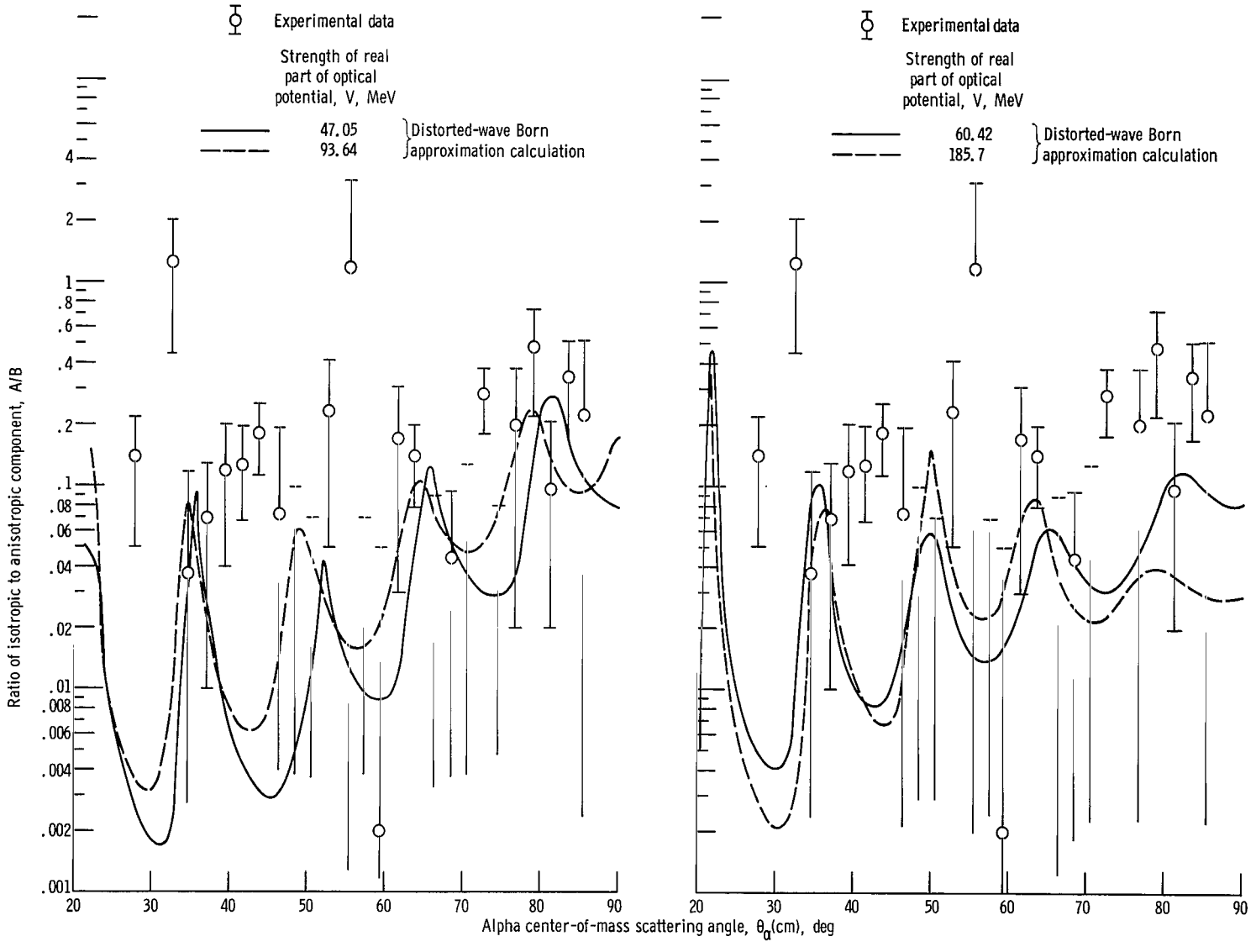

(a) First and second sets of optical potentials.

(b) Third and fourth sets of optical potentials.

Figure 7. - Comparison of measured and calculated values of ratio of isotropic to anisotropic component for the reaction $^{24}Mg(\alpha, \alpha'\gamma)$.

$$\left.\begin{aligned} \alpha &= \alpha' \\ \beta &= 1.154\,\beta' \\ \gamma &= 1.154\,\gamma' \end{aligned}\right\} \tag{4}$$

The true A, B, and θ_o are then related to α, β, and γ by the expressions

$$A = \alpha - \sqrt{\beta^2 + \gamma^2}$$

$$B = +2\sqrt{\beta^2 + \gamma^2}$$

$$\theta_o = \frac{1}{4}\arctan\frac{\gamma}{\beta}$$

Thus, the symmetry angle of the correlation pattern θ_o is unchanged by the finite size correction, whereas the ratio A/B is decreased somewhat.

A list of the experimental results for the parameters A/B and θ_o are given in table I. These same quantities are shown graphically as a function of alpha scattering angle in figures 6 and 7.

THEORY

Distorted-Wave Born Approximation Theory of Inelastic Scattering

The inelastic scattering of 42- to 43- MeV alpha particles from ^{24}Mg has been analyzed by Rost and Austern (ref. 11) and by Bassel, et al. (ref. 12) using the distorted-wave Born approximation. These authors assumed that the inelastic scattering to the 2^+ state of ^{24}Mg results from a collective excitation. Analysis of the angular correlation in the reaction ^{24}Mg $(\alpha, \alpha'\gamma)$ ^{24}Mg provides additional evidence for the collective nature of this transition.

The distorted-wave Born approximation transition amplitude for inelastic scattering to collective states has been calculated by various authors (refs. 5 and 12). It is assumed that the potential strength depends only on the distance of the particle from the nuclear surface and that the optical potential has, in addition to the spherical part, nonspherical components which give rise to inelastic scattering. The general procedure

is to expand the optical potential about its spherical potential and retain only first-order terms in the deformation. Ordinarily, the parameters which determine the spherical part of the potential are determined by fitting elastic scattering from the same nucleus. The general expression for the transition amplitude is

$$T_{fi} = \langle \varphi_f \chi_f^{(-)} | V_1 | \varphi_i \chi_i^{(+)} \rangle \tag{5}$$

where V_1 is that part of the optical potential which is nonspherical; $\chi_i^{(+)}$ and $\chi_f^{(-)}$ are the distorted waves in the incoming and outgoing channels, respectively; and φ_i and φ_f are the initial and final states of the nucleus. For the sake of completeness, the expressions for T_{fi}, the angular distributions, and the angular correlation are given as follows:

$$T_{fi} = \sum_{L_1 \mu_1} \langle JM, L_1 \mu_1 | J'M' \rangle \, Q_{L_1} F_{L_1}{}^{\mu} F_{L_1 \mu_1} \tag{6}$$

where J and J' are the total spins of the initial and final states of the nucleus, M and M' are their respective projections,

$$Q_{L_1} = \left(\frac{2J+1}{2J'+1} \right)^{1/2} \langle JM, \, L_1 0 | J'M \rangle$$

$$F_{L_1 \mu_1} = \sum_{L\ell} \Gamma_{L\ell}^{L_1 \mu_1} F_{L_1}(L\ell) P_L^{|\mu_1|}(\cos \theta)$$

where

$$\Gamma_{L\ell}^{L_1 \mu_1} = \sqrt{4\pi} \, i^{(\ell - L - \mu_1 + |\mu_1|)} (2L+1)(2\ell+1)(2L_1+1)^{1/2}$$

$$\times \left[\frac{(L - |\mu_1|)!}{(L + |\mu_1|)!} \right]^{1/2} \langle L\mu_1, \ell 0 | L_1 \mu_1 \rangle \langle L0, \ell 0 | L_1 0 \rangle$$

and

$$F_{L_1}(L\ell) = \int_0^\infty f_L(k_f r) v_{L_1}(r) f_\ell(k_i r) r^2 dr$$

where the $f_L(kr)$ are the partial wave components of the distorted waves, and $v_{L_1}(r)$ is the surface interaction form factor. When the spherical part of the optical potential is of the Woods-Saxon form

$$U_{opt}(r) = (V + iW)f(r)$$

where

$$f(r) = \left[1 + \exp\left(\frac{r - R_s}{a_s}\right)\right]^{-1}$$

then

$$v_{L_1}(r) = \left(\frac{V_0 R_s}{a_s}\right)\left[2 + \exp\left(\frac{r - R_s}{a_s}\right) + \exp\left(\frac{-r + R_s}{a_s}\right)\right]^{-1} \tag{7}$$

where R_s is the radius of the surface interaction form factor, a_s is the diffuseness, and V_0 is the strength of the interaction.

The differential scattering cross section is given by

$$\frac{d\sigma}{d\Omega} = \sum_{\mu_1} \frac{|F_{L_1\mu_1}|^2}{2L_1 + 1} \tag{8}$$

It should be noted here that since only the squares of the direct reaction amplitudes appear in the summation, the differential cross section will be insensitive to the phases of the amplitudes. The angular correlation of the deexcitation gamma rays with the inelastically scattered alpha particles is

$$W(\Omega_{k_f}^{\rightarrow}, \Omega_\gamma) = \sum_{\substack{\mu_1 \mu_1' \\ \lambda\mu}} F^*_{L_1\mu_1} F_{L_1\mu_1'} \langle 2\lambda\mu, L_1\mu_1' | L_1\mu_1 \rangle \langle L_1 1, L_1 - 1 | 2\lambda, 0 \rangle \, Y^{\mu}_{2\lambda}(\Omega_\gamma) \quad (9)$$

where $\Omega_{k_f}^{\rightarrow}$ and Ω_γ refer to the directions of the scattered alpha particle and gamma ray, respectively, and a transition of the type $0^+ \rightarrow L_1^+ \rightarrow 0^+$ has been assumed. Clearly, the angular correlation will be sensitive to the phases of the direct reaction amplitudes. For the case of $L_1 = 2$, which is considered here, Banerjee and Levinson (ref. 13) have shown that the angular correlation in the reaction plane can be written

$$W(\theta_\alpha, \theta_\gamma) = A + B \sin^2 2(\theta_\gamma - \theta_o) \quad (10)$$

where θ_o is the symmetry angle; A, B, and θ_o are functions of the scattering angle θ_α.

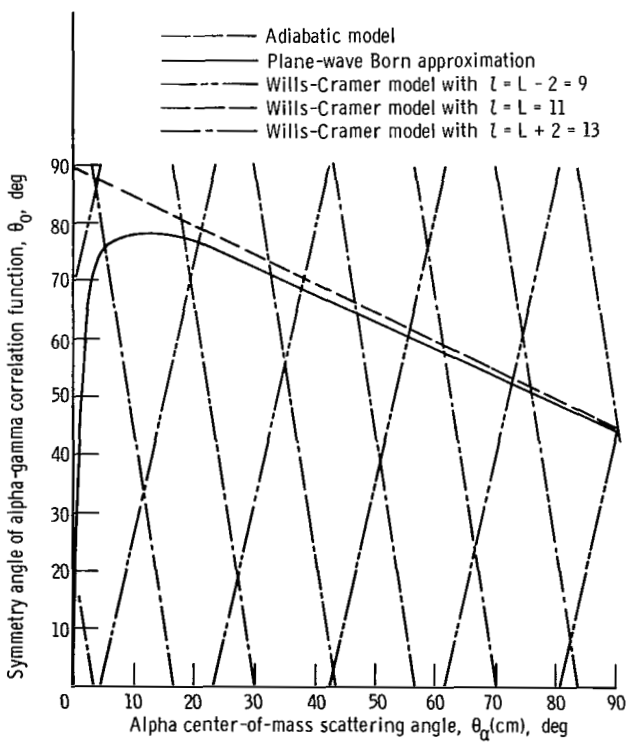

Figure 8. - Symmetry angle as predicted by adiabatic approximation, plane-wave Born approximation, and Wills-Cramer. It should be noted that the predictions of the adiabatic model are identical to those of the Wills-Cramer model with $l = L$.

Adiabatic Approximation and Plane-Wave Born Approximation

Blair and Wilets (ref. 6) calculated the correlation pattern as a function of alpha scattering angle in the adiabatic approximation. They obtained the result

$$W(\theta_\alpha, \theta_\gamma) = B \sin^2 2(\theta_\gamma - \theta_R)$$

where θ_R is the angle of adiabatic recoil of the target nucleus. This angle varies linearly from 90° to 0° as the scattering angle goes from 0° to 180°. The prediction of the plane-wave Born approximation (ref. 14) is almost identical except that the symmetry angle follows the nonadiabatic recoil direction of the target nucleus. These two angles differ by less than 5° for scattering greater than 15°. Both predictions are shown in figure 8.

Wills-Cramer Model

Wills and Cramer (ref. 7) have proposed a simple model to explain the 22-MeV carbon and magnesium data. They assume that only one incoming (L) and one outgoing (l) wave are responsible for the interaction. In this approximation, the symmetry angle is predicted to be

$$\theta_o = \frac{1}{4}\left[(2l + 1)\theta_\alpha - \frac{\pi}{2}\right] \qquad \text{for } l = L - 2 \tag{11}$$

or

$$\theta_o = \frac{\pi}{2} - \frac{1}{2}\theta_\alpha \qquad \text{for } l = L \tag{12}$$

or

$$\theta_o = -\frac{1}{4}\left[(2l + 1)\theta_\alpha - \frac{\pi}{2}\right] \qquad \text{for } l = L + 2 \tag{13}$$

These three predictions are illustrated in figure 8. The expression of equation (12) is identically equal to the adiabatic prediction.

ANALYSIS OF ANGULAR CORRELATION

Distorted-Wave Born Approximation

The principal difficulty involved in the distorted-wave Born approximation analysis of the angular correlation data (and the elastic and inelastic scattering as well) is the ambiguity which exists in the optical model parameters. This has been investigated in some detail by Drisko, et al. (ref. 15), and for heavier isotopes by Leonard, Baron, and Stewart (ref. 9) and Bingham, Halbert, and Bassel (ref. 16). In the present case,

TABLE II. - MAGNESIUM 24 OPTICAL POTENTIALS

Set	Nuclear radius constant, R_o, fm	Strength of real part of optical potential, V, MeV	Strength of imaginary part of optical potential, W, MeV	Diffuseness parameter, a, fm	Goodness of fit, χ^2/N	Total reaction cross section, σ_R, $(fm)^2$	Nuclear deformation parameter, β_2
1	1.635	47.05	21.11	0.5613	31.8	117.9	0.58
2	1.49	93.64	31.12	.6190	55.9	123.1	.56
3	1.53	60.42	25.58	.6511	31.5	123.1	.59
4	1.38	185.7	42.50	.5753	24.1	117.6	.59
5	1.71	38.85	18.21	.5063	34.9	116.2	---
6	1.595	51.55	22.64	.5972	31.7	119.8	---
7	1.42	124.5	36.28	.6109	26.8	119.8	0.68
8	1.34	195.1	46.28	.5966	25.2	117.8	.60

as in others, several sets of parameters have been found which yield equivalently good fits to the elastic scattering (see table II). Four sets of these parameters will be presented for a detailed comparison with the experimental data. Comparison with the elastic cross section data (ref. 17) is shown in figure 9. For all four potentials, agreement is rather good at forward angles ($\theta < 90^o$) and less satisfactory at larger angles.

Calculated inelastic cross sections are compared with the experimental data (ref. 17) in figure 10. These results were obtained by using the first four sets of optical model parameters listed in table II, together with the Direct Reaction Calculation program of Gibbs, et al. (ref. 18). The interaction form factor for the calculation was a derivative Woods-Saxon, peaked at the radius of the optical potential. The agreement between theory and inelastic scattering is not particularly good. Although the pre-

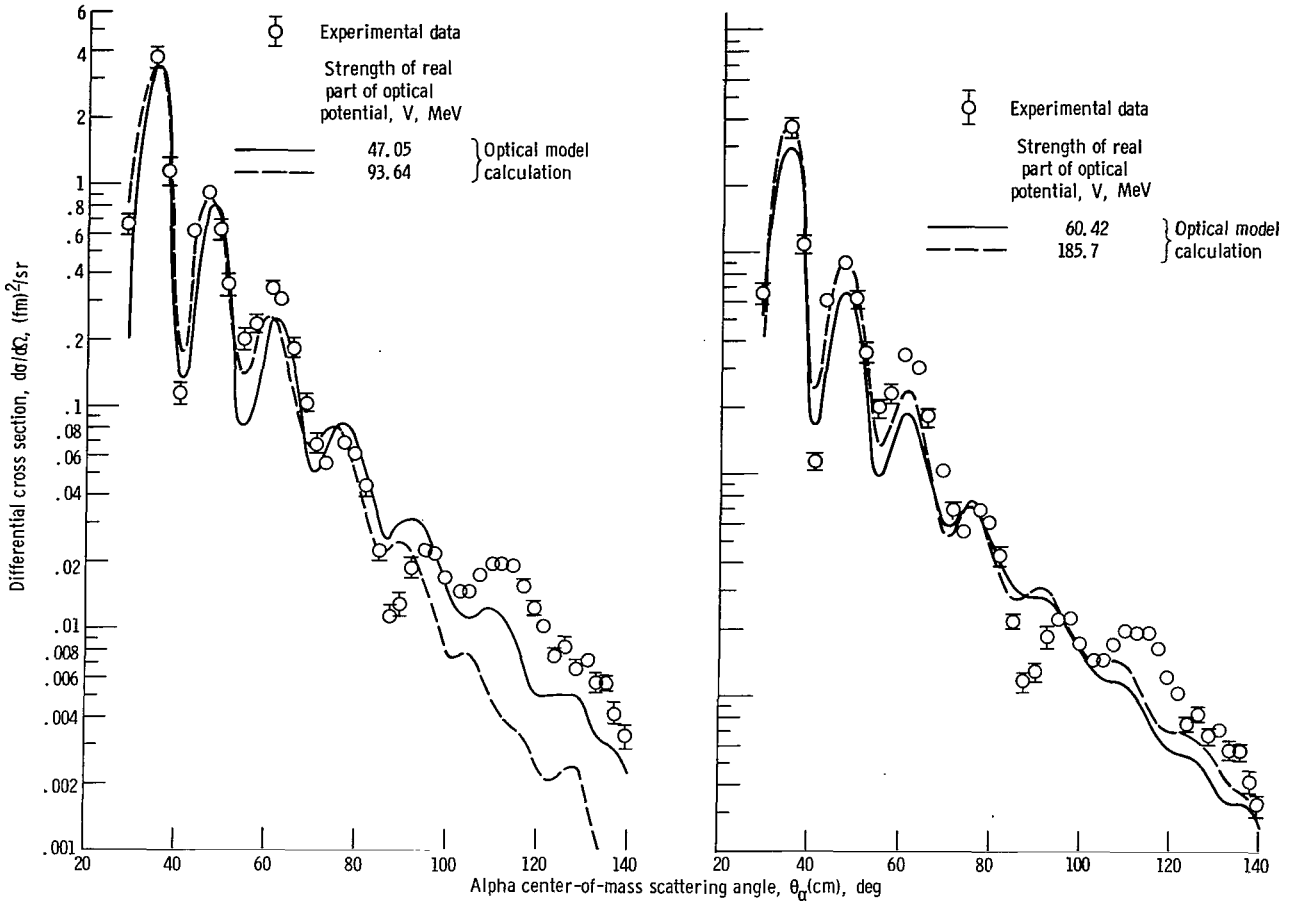

(a) First and second sets of optical potentials.

(b) Third and fourth sets of optical potentials.

Figure 9. - Experimental and theoretical cross sections for elastic scattering of 42-MeV alpha particles from magnesium 24.

dicted maxima and minima fall in the proper places, the experimental data do not fall quite as rapidly as the theoretical curves. Normalization of theoretical to experimental data was performed in every case at $\theta_\alpha = 40^\circ$ and made possible the extraction of a deformation parameter β_2 for each optical potential. These are listed in table II and are all seen to be similar to each other and in agreement with the value previously reported (ref. 19).

The results of the $\alpha, \alpha'\gamma$ experiment are shown in figures 6 and 7. In figures 6(a) and 7(a), the lines results from the first two sets of optical potentials; in figures 6(b) and 7(b) they result from the third and fourth sets. For scattering angles greater than 25°, all four of these potentials (as well as the four not explicitly shown) predict nearly the same behavior for the symmetry angle. They are in qualitative agreement with the data, predicting small fluctuations about the adiabatic line with no rapid rotations of the gamma pattern. The observed behavior is similar, but the experimental symmetry angle is generally smaller by about 5°.

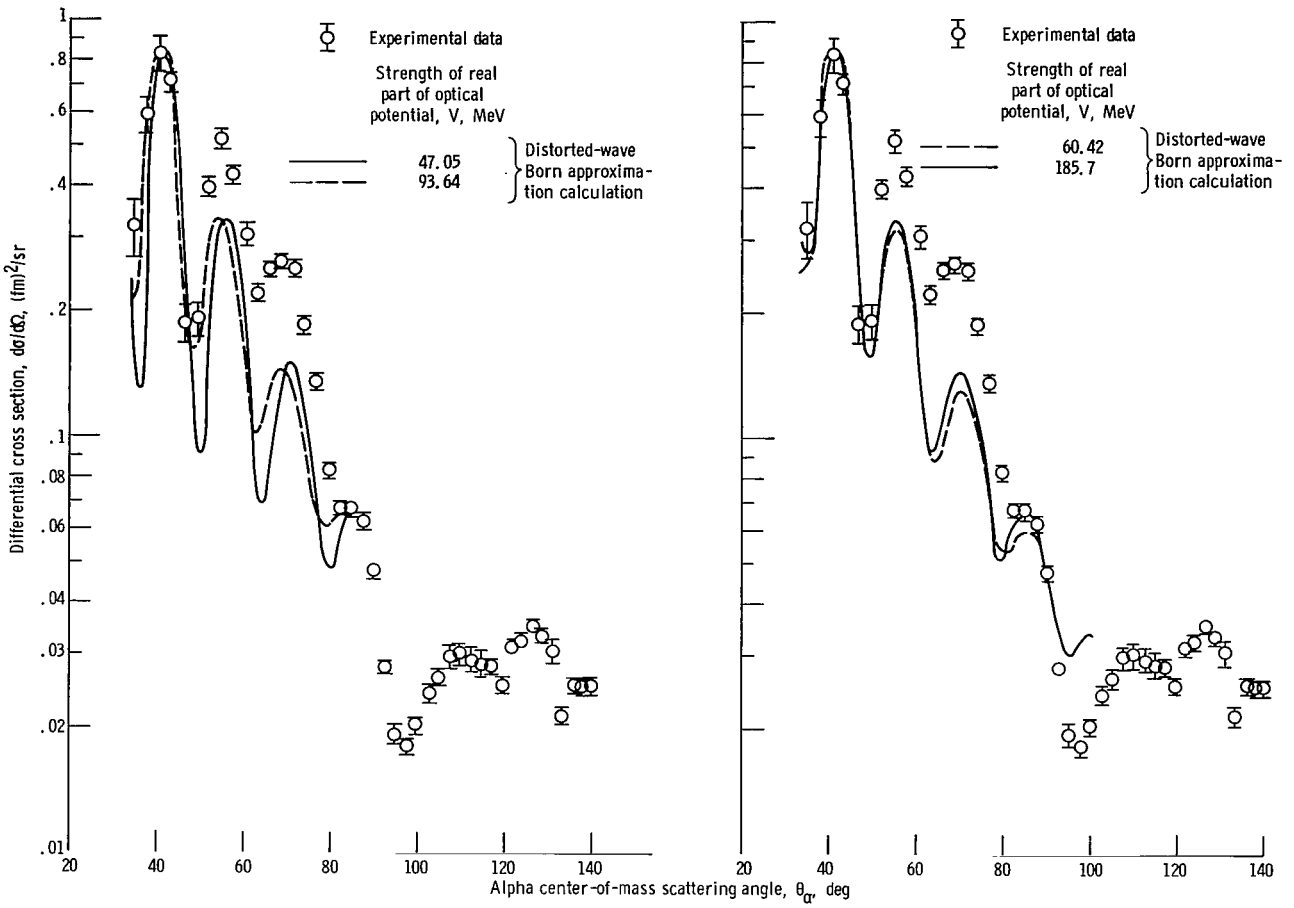

(a) First and second sets of optical potentials.

(b) Third and fourth sets of optical potentials.

Figure 10. - Experimental and theoretical cross sections for inelastic scattering of 42-MeV alpha particles from the 1.37-MeV state of magnesium 24.

Forward of 25°, only one optical potential predicts the rapid rotation of the gamma pattern which is observed by Hendrie (refs. 2 and 3) near 20°. This is set I of table II, which has V = 47.05 MeV. This potential is very similar to that which Hendrie used. All other potentials examined predicted a reversal of the direction of rotation of the gamma pattern at $\theta = 20^{\circ}$, in conflict with the experimental results.

The calculated A/B ratios are shown with the data in figure 7. In spite of the large errors of the experimental data, the calculated values are in serious disagreement forward of $\theta_{\alpha} = 50^{\circ}$. At larger angles, however, the average behavior of A/B is reproduced, if not the details.

Other Models

It is clear from figure 8 that none of the simpler models is adequate for predicting the behavior of the correlation pattern over the angular range for which data are available. The adiabatic and plane-wave Born approximations do not predict any of the rapid reverse rotations seen at forward angles, while the Wills-Cramer model does not predict the damping of the rotation seen at alpha scattering angles larger than 30^{o}.

DISCUSSION AND CONCLUSIONS

It is clear that the data obtained in the present experiment differ qualitatively from those which have been obtained in previous experiments (refs. 1 to 3). In the work with 22.5-MeV alpha particles, a continuous rotation of the gamma pattern was observed for alpha scattering angles between 20^{o} and 100^{o}. Only at approximately 100^{o} does the first reversal of the direction of rotation occur. The same is true of the forward angle data of Hendrie (refs. 2 and 3) displayed in figure 6. At angles forward of 30^{o}, the gamma pattern rotates continuously in the same direction. At 35^{o} it is not clear whether the pattern continues to rotate or reverses. Beyond 35^{o}, the region examined here, it is clear that there is not rapid rotation, but only a slow variation, approximately as predicted in the adiabatic approximation.

The analysis of the reaction studied here is based primarily on the distorted-wave Born approximation theory of inelastic scattering, with the assumption that the ^{24}Mg nucleus is described by the macroscopic collective model. The results so obtained agree moderately well with experiment.

Examination of the elastic scattering (fig. 9) indicates rather clearly that there are many sets of optical potentials which yield comparable results when compared with experiment. This, however, is not surprising in view of the discussion given in the distorted-wave Born approximation section of the analysis.

The distorted-wave Born approximation predictions for the inelastic scattering (fig. 10) are similar in quality to the elastic fits. All yield a value of the deformation parameter which is in reasonable agreement with the accepted value of 0.65; all have similar shapes and are not in very good agreement with the experimental data. This is similar to the findings of reference 9.

The results of the angular correlation study are shown in figures 6 and 7. The predictions for the A/B ratio are in poor agreement for all the potentials tested. The symmetry angle on the other hand is reasonably well predicted by all the potentials. All predict a rapid rotation at the forward angles and small oscillations about the

adiabatic line at angles beyond 35°. All differ from the data by approximately 5° to 10° for alpha scattering angles larger than about 45°. This would indicate that angular correlation studies are not nearly so sensitive as was hoped to the variation of the optical model parameters. In fact the only real difference which could be observed in the predictions of the various optical potentials was that one of them (V = 47.05-MeV) was able to reproduce the rapid rotation observed by Hendrie in the neighborhood of $\theta_{\alpha} = 21^{\circ}$. At all other angles, however, the predictions of this potential are equivalent to all the others.

Two conclusions may be drawn from this study. First, although one of the optical potentials (V = 47.05 MeV) was somewhat better than the others, the overall predictions for the behavior of the gamma ray symmetry angle was not nearly so sensitive to the variation of optical model parameters as was hoped. Second, none of the optical potentials provided a really good description of the behavior of the correlation pattern. Particularly poor agreement was obtained for the A/B ratios. This indicates that either a more detailed reaction calculation (coupled channels) or a more detailed model of the nucleus is required. It has been shown (refs. 2 and 3) that a coupled-channels calculation can improve the fit to the inelastic cross section, but that it does not seem to help the angular correlation results. A more detailed model of the ^{24}Mg nucleus would take into account the interaction of the projectile (alpha particle) with each of the nucleons in the nucleus. If such a model were successful in distorted-wave Born approximation studies, it could be built into the coupled-channels formalism. A calculation of this type would be the most complete possible with the present knowledge of nuclear structure and nuclear reactions.

Lewis Research Center,
National Aeronautics and Space Administration,
Cleveland, Ohio, April 10, 1968,
129-02-04-06-22.

REFERENCES

1. Eidson, W. W.; Cramer, J. G., Jr.; Blatchley, D. E.; and Bent, R. D.: Angular Correlation Studies of Nuclear Polarization Following Inelastic Scattering of Alpha Particles From C^{12} and Mg^{24}. Nucl. Phys., vol. 55, no. 4, 1964, pp. 613-642.

2. Farwell, G. W.; Hendrie, D. L.; and Peterson, R. J.: Alpha-Gamma Correlations on Mg^{24}. Annual Rep., Univ. Washington, Nuclear Physics Lab., 1965, pp. 25-27.

3. Hendrie, David L.: A Study of Coincidences Between Inelastically Scattered 42-MeV Alpha Particles and De-excitation Gamma Rays. Ph.D. Thesis, Univ. Washington, 1964.

4. Hodgson, Peter E.: The Optical Model of Elastic Scattering. Oxford Univ. Press, 1963.

5. Tobocman, W.: Theory of Direct Nuclear Reactions. Oxford Univ. Press, 1961.

6. Blair, J. S.; and Wilets, L.: Gamma-Ray Correlation Function in the Adiabatic Approximation. Phys. Rev., vol. 121, no. 5, Mar. 1, 1961, pp. 1493-1499.

7. Wills, J. G.; and Cramer, J. G., Jr.: Angular Momentum Selection and Angular Correlations in Direct Reactions with Strongly Absorbed Particles. Nuclear Spectroscopy with Direct Reactions. I. Contributed Papers, F. E. Throw, ed. Rep. No. ANL-6848, Argonne National Lab., Mar. 1964, pp. 147-152.

8. Baron, Norton; and Kaminski, Gerald A.: Manufacture of Lithium-Drifted Silicon Surface-Barrier Semiconductor Counters. NASA TN D-3554, 1966.

9. Leonard, R. F.; Stewart, W. M.; and Baron, N.: Alpha-Particle Scattering From Even Tellurium Isotopes. Phys. Rev., vol. 162, no. 4, Oct. 20, 1967, pp. 1125-1129.

10. Rose, M. E.: The Analysis of Angular Correlation and Angular Distribution Data. Phys. Rev., vol. 91, no. 3, Aug. 1, 1953, pp. 610-615.

11. Rost, E.; and Austern, N.: Inelastic Diffraction Scattering. Phys. Rev., vol. 120, no. 4, Nov. 15, 1960, pp. 1375-1387.

12. Bassel, R. H.; Satchler, G. R.; Drisko, R. M.; and Rost, E.: Analysis of the Inelastic Scattering of Alpha Particles. I. Phys. Rev., vol. 128, no. 6, Dec. 15, 1962, pp. 2693-2707.

13. Banerjee, Manoj K.; and Levinson, Carl A.: Direct Interaction Theory of Inelastic Scattering. Part II. Angular Correlation of Gamma Rays Following Inelastic Scattering. Ann. Phys. (N.Y.), vol. 2, no. 5, Nov. 1957, pp. 499-524.

14. Satchler, G. R.: Gamma Radiation Following the Surface Scattering of Nucleons. Proc. Phys. Soc., vol. A68, pt. 11, Nov. 1955, pp. 1037-1040.

15. Drisko, R. M.; Satchler, G. R.; and Bassel, R. H.: Ambiguities in the Optical Potential for Strongly Absorbed Projectiles. Phys. Letters, vol. 5, no. 5, Aug. 1, 1963, pp. 347-350.

16. Bingham, C. R.; Halbert, M. L.; and Bassel, R. H.: Nuclear-Reaction Studies with 65-MeV Alpha Particles on Zirconium. Phys. Rev., vol. 148, no. 3, Aug. 19, 1966, pp. 1174-1191.

17. Vincent, J. S.; Boschitz, E. T.; and Priest, J. R.: Large Angle Alpha Particle Scattering from the 3^+ Unnatural Parity States in Magnesium. Phys. Letters, vol. 25B, no. 2, Aug. 7, 1967, pp. 81-83.

18. Gibbs, W. R.; Madsen, V. A.; Miller, J. A.; Tobocman, W.; Cox, E. C.; and Mowry, L.: Direct Reaction Calculation. NASA TN D-2170, 1964.

19. Way, K., ed.: Nuclear Transition Probability B(E2) for $0^+_{g.s.}$ - 2^+_{first} Transitions and Deformation Parameter, β_2. Nucl. Data, Sec. A, vol. 1, no. 1, Dec. 1965, pp. 21-102.

"The aeronautical and space activities of the United States shall be conducted so as to contribute . . . to the expansion of human knowledge of phenomena in the atmosphere and space. The Administration shall provide for the widest practicable and appropriate dissemination of information concerning its activities and the results thereof."

—NATIONAL AERONAUTICS AND SPACE ACT OF 1958

NASA SCIENTIFIC AND TECHNICAL PUBLICATIONS

TECHNICAL REPORTS: Scientific and technical information considered important, complete, and a lasting contribution to existing knowledge.

TECHNICAL NOTES: Information less broad in scope but nevertheless of importance as a contribution to existing knowledge.

TECHNICAL MEMORANDUMS: Information receiving limited distribution because of preliminary data, security classification, or other reasons.

CONTRACTOR REPORTS: Scientific and technical information generated under a NASA contract or grant and considered an important contribution to existing knowledge.

TECHNICAL TRANSLATIONS: Information published in a foreign language considered to merit NASA distribution in English.

SPECIAL PUBLICATIONS: Information derived from or of value to NASA activities. Publications include conference proceedings, monographs, data compilations, handbooks, sourcebooks, and special bibliographies.

TECHNOLOGY UTILIZATION PUBLICATIONS: Information on technology used by NASA that may be of particular interest in commercial and other non-aerospace applications. Publications include Tech Briefs, Technology Utilization Reports and Notes, and Technology Surveys.

Details on the availability of these publications may be obtained from:

SCIENTIFIC AND TECHNICAL INFORMATION DIVISION

NATIONAL AERONAUTICS AND SPACE ADMINISTRATION

Washington, D.C. 20546